

# CHANDRA/HETGS SPECTROSCOPY OF THE GALACTIC BLACK HOLE GX 339–4: A RELATIVISTIC IRON EMISSION LINE AND EVIDENCE FOR A SEYFERT-LIKE WARM ABSORBER

J. M. MILLER<sup>1,2</sup>, J. RAYMOND<sup>1</sup>, A. C. FABIAN<sup>3</sup>, J. HOMAN<sup>4</sup>, M. A. NOWAK<sup>5</sup>, R. WIJNANDS<sup>6</sup>, M. VAN DER KLIS<sup>7</sup>, T. BELLONI<sup>4</sup>, J. A. TOMSICK<sup>8</sup>, D. M. SMITH<sup>9</sup>, P. A. CHARLES<sup>10</sup>, W. H. G. LEWIN<sup>5</sup>,

*Subject headings:* Black hole physics – relativity – stars: binaries (GX339–4) – stars: binaries (XTE J1650–500)  
– physical data and processes: accretion disks

*Draft version February 7, 2020*

## ABSTRACT

We observed the Galactic black hole GX 339–4 with the *Chandra* High Energy Transmission Grating Spectrometer (HETGS) for 75 ksec during the decline of its 2002–2003 outburst. The sensitivity of this observation provides an unprecedented glimpse of a Galactic black hole at about a tenth of the luminosity of the outburst peak. The continuum spectrum is well described by a model consisting of multicolor disk blackbody ( $kT \simeq 0.6$  keV) and power-law ( $\Gamma \simeq 2.5$ ) components. X-ray reflection models yield improved fits. A strong, relativistic Fe  $K\alpha$  emission line is revealed, indicating that the inner disk extends to the innermost stable circular orbit. The line is not sufficiently broad to strongly require black hole spin. Absorption lines from H-like and He-like O, and He-like Ne and Mg are detected, as well as lines which are likely due to Ne II and Ne III. The measured line properties make it difficult to associate the absorption with the coronal phase of the interstellar medium. A scenario wherein the absorption lines are due to a local AGN-like warm-absorber geometry — perhaps produced by a disk wind in an extended disk-dominated state — may be more viable. We compare our results to *Chandra* observations of the Galactic black hole candidate XTE J1650–500, and discuss our findings in terms of prominent models for Galactic black hole accretion flows and connections to supermassive black holes.

## 1. INTRODUCTION

The low mass X-ray binary (LMXB) GX 339–4 has been a very important object in the study of Galactic black hole candidates (BHC), owing to several interesting properties. It is a quasi-persistent/recurring transient source, and therefore historically it has transited through a wide range of luminosities and X-ray spectral states (Ilovaisky et al. 1986, Grebenev et al. 1991, Miyamoto et al. 1991, Mendez & van der Klis 1997, Belloni et al. 1999). The classification of GX 339–4 as a BHC arose because its X-ray spectral and timing behavior was very similar to that of dynamically determined BHCs (e.g., Nova Muscae 1991, Miyamoto et al. 1993). Recently, Hynes et al. (2003) have used high resolution optical spectroscopy of Bowen fluorescence lines from the secondary to arrive at a mass of  $M_{BH} = 5.8 \pm 0.5 M_{\odot}$  which clearly establishes the black hole nature of the primary in GX 339–4.

Further interest in GX 339–4 is owed to the fact that the broad-band spectrum, from radio through gamma-ray wavelengths, is likely dominated by emission from the accretion flows around the central compact object. The secondary makes little contribution to the spectrum. It had been suggested, partly based upon possible fast time scale X-ray/optical correlations (e.g. Motch et al. 1983), that even the optical emission in the

spectrally hard/high variability X-ray ‘low state’ was due to synchrotron emission from an extended outflow near the compact object (Fabian et al. 1982, Imamura et al. 1990, Steiman et al. 1990). Evidence of a jet-like outflow in the low-luminosity X-ray hard state was strengthened by the detection of radio emission at  $\approx 3$ –10 mJy levels that is positively correlated with the hard state X-ray flux (Fender et al. 1999, Wilms et al. 1999). At the opposite extreme of X-ray flux, the spectrally soft and moderately variable ‘very high state’ was first recognized as a state with distinct properties in GX 339–4 (Miyamoto et al. 1991); later it was also realized that outflows may occur in this state (Miyamoto et al. 1995).

Fluorescent Fe  $K\alpha$  line emission can be a very powerful probe of the accretion flow geometry in Galactic black holes. Such lines are very likely produced through irradiation of the inner accretion disk; therefore, the breadth of such lines can serve as a trace of the inner disk extent. A primary prediction of advection-dominated accretion flow (ADAF) models (see, e.g., Esin, McClintock, & Narayan 1997) is that the accretion disk should radially recede as the mass accretion rate ( $\dot{m}$ ) falls. Following a long outburst of GX 339–4 in 2002–2003, we requested and were granted a Director’s Discretionary Time observation with *Chandra* in part to test this prediction as the out-

<sup>1</sup>Harvard-Smithsonian Center for Astrophysics, 60 Garden Street, Cambridge, MA 02138, jmmiller@cfa.harvard.edu

<sup>2</sup>NSF Astronomy and Astrophysics Fellow

<sup>3</sup>Institute of Astronomy, University of Cambridge, Madingley Road, Cambridge CB3 0HA, UK

<sup>4</sup>INAF – Osservatorio Astronomico di Brera, Via E. Bianchi 46, 23807 Merate, IT

<sup>5</sup>Center for Space Research and Department of Physics, Massachusetts Institute of Technology, Cambridge, MA 02139–4307

<sup>6</sup>School of Physics and Astronomy, University of St. Andrews, North Haugh, St. Andrews Fife, KY16 9SS, UK

<sup>7</sup>Astronomical Institute “Anton Pannekoek,” University of Amsterdam, and Center for High Energy Astrophysics, Kruislaan 403, 1098 SJ, Amsterdam, NL

<sup>8</sup>Center for Astrophysics and Space Sciences, Code 0424, University of California, San Diego, La Jolla, CA 92093

<sup>9</sup>Space Sciences Laboratory, University of California, Berkeley, Centennial at Grizzly Park Boulevard, Berkeley, CA, 94720-7450

<sup>10</sup>Department of Physics and Astronomy, University of Southampton, SO17 1BJ, UK

burst decayed. Although prior observations have found broad lines suggesting that the disk remains close to the innermost stable circular orbit (ISCO) in GX 339-4 both in rather bright phases and deep in the low/hard state (see, e.g., Nowak et al. 2002), such observations were limited by coarse spectral resolution and sensitivity. In contrast, the resolution of the *Chandra* High Energy Transmission Grating Spectrometer (HETGS) allows broad Fe  $K\alpha$  emission lines to clearly be revealed as intrinsically broad (Miller et al. 2002a).

A second important motivation for our observation was to search for evidence of a disk-driven outflow. Preliminary indications for absorption lines from low-Z elements in a BHC — perhaps due to such an outflow — were first seen in two *Chandra*/HETGS observations of the BHC XTE J1650-500 (Miller et al. 2002b). There is ample observational evidence to suggest that such an outflow should exist in Galactic black hole systems: a disk wind has been dramatically revealed in the neutron star system Circinus X-1 (Brandt & Schulz 2000), and disk-driven outflows may be common in AGN (Elvis 2000, Morales & Fabian 2002, Turner et al. 2003). With gratings covering the 0.5–10.0 keV band, the *Chandra*/HETGS is well suited to searching for lines from low-Z elements and lines due to Fe L-shell transitions.

## 2. OBSERVATION AND DATA REDUCTION

GX 339-4 was observed with *Chandra* for approximately 75 ksec, starting on UT 2003 March 17.8. The HETGS-dispersed spectrum was read out with the ACIS-S array operating in timed exposure (TE) mode. A 400-row subarray was used to reduce the frametime to  $(400/1024) \times 2.5\text{s} \simeq 1.0\text{s}$ ; a negative consequence of this action is that the MEG spectra are truncated just below the O edge energy (the O edge occurs 0.53 keV and is due to photoelectric absorption in the interstellar medium, or ISM). A Y-coordinate translation of +0.33 arcmin was used to move chip gaps that might fall in the red wing of a broad Fe  $K\alpha$  emission line in the first-order HEG spectra to the 9.5–10.5 keV range.

Apart from this observation of GX 339-4, the most sensitive *Chandra* spectra of an LMXB BHC were obtained through observations of XTE J1650-500. XTE J1650-500 was observed with the *Chandra*/HETGS on two occasions for 30 ksec each. The first observation started on UT 2001 October 5.9, and the second observation started on UT 2001 October 29.0. The HETGS-dispersed spectrum was read-out with the ACIS-S array operating in continuous clocking (CC) mode to avoid photon pile-up. A “gray” filter (1 in 10 events were telemetered in a region 100 columns wide) was put into effect in the region of the zeroth order to also avoid telemetry saturation. To avoid any wear and tear on the nominal ACIS-S3 aimpoint while keeping as much of the HEG Fe  $K\alpha$  line region on the backside-illuminated ACIS-S3 chip, the nominal aimpoint was moved 4.0mm toward the top of the ACIS-S array, and a Y translation of -1.33 arcmin was made. These steps were likely overly conservative, and had the negative consequence of placing chip gaps in the red wing of any broad Fe  $K\alpha$  emission line. Inspection of the data reveals gain variations and/or CTI effects across some of the chips that are not fully accounted for by the current calibration.

The *Chandra* datasets were reduced using tools in the CIAO version 2.3 analysis suite. The highest level filtered event list (evt2) was further refined by running the tool “destreak” on the ACIS-S4 chip to remove detector effects. Spectra

were extracted at the nominal instrumental resolution (HEG: 0.0025 Å, MEG: 0.005 Å) using the tool “tgextract”. Source and background spectra were extracted using the nominal regions. Standard redistribution matrix files (rmfs) from the CALDB database were used to generate ancillary response files (arfs) and for spectral fitting; arf files were made using the script “fullgarf”. Lightcurves of the dispersed counts were made using the tool “lightcurve”.

Only background-subtracted spectra were considered for analysis; nominal background regions were selected during the source spectrum extraction. The high-resolution spectra were analyzed using ISIS version 1.0.50 (Houck & Denicola 2000). Analysis of the broad-band spectrum and Fe  $K\alpha$  emission line was made using XSPEC version 11.2 (Arnaud & Dorman 2000). After inspecting the first-order spectra individually, the background-subtracted first-order MEG spectra and arfs were added using the tool “add\_grating\_spectra” prior to analysis; the same procedure was performed on the background-subtracted first-order HEG spectra and arfs.

## 3. ANALYSIS AND RESULTS

The lightcurve of the dispersed spectrum of GX 339-4 is remarkably constant (see Fig. 1), and so we consider the time-averaged spectra for analysis. The MEG spectra are more sensitive below 2 keV, however deviations are clear below 1 keV which are likely due to the well-documented carbon build-up on the ACIS detectors. At the time of writing, there is no way to correct for this effect in grating spectra. Examining the individual ISM photoelectric absorption edges in the source spectrum with local models consisting only of power-law continua with simple edge functions, we find that the neutral (atomic) O, Fe L3 and L2, Ne, Mg, and Si edges indicate abundances of 0.75–1.0 (relative to Solar) along this line of sight. We regard these measurements with caution, however. Not only is the effective area below 1 keV affected by the carbon build-up, but the Si range is distorted by an “inverse edge” near 2.07 keV, likely due to the Ir coating on the mirrors. Due to these calibration uncertainties, we have characterized the broad-band continuum properties using the HEG spectra as their broader energy range should limit the relative importance of these systematic effects. The MEG spectra were used to characterize the soft X-ray absorption lines discovered in the spectra due to its higher effective area in the energy range of interest.

### 3.1. The Continuum Spectrum and Relativistic Fe $K\alpha$ Emission Line

Initial fits revealed that the combined HEG spectrum is robust in the 1.2–10.0 keV range. Nominally, HEG spectra are robust in the 0.8–10.0 keV range; however, our 400-row subarray causes the spectra to be truncated near 1.2 keV. For consistency, the spectra from XTE J1650-500 were also fit only in this range. In all fits, an inverse edge was included at 2.07 keV with  $\tau = -0.13$ . This value for  $\tau$  is largely model-independent, and effectively corrects the Ir calibration error.

The results of all broad-band spectral fits are listed in Table 1. We fit the standard multicolor disk (MCD) blackbody plus power-law model to each of the source spectra, modified by photoelectric absorption in the ISM (using the “phabs” model in XSPEC). In all fits, the power-law index was constrained to be within  $\Delta(\Gamma) \leq 0.2$  of the value measured via fits to simultaneous *RXTE* spectra in the 3–200 keV band. Joint fits to the simultaneous *Chandra* and *RXTE* spectra will be presented in separate work. Unabsorbed fluxes were calculated on the

standard 0.5–10.0 keV band to best correspond to other *Chandra* and *XMM-Newton* LMXB and BHC observations made using more common instrumental offsets and parameters. The spectra of XTE J1650–500 are affected by chip gaps below the Fe K $\alpha$  emission line range due to the Y-offset chosen for these observations, and so we only characterize the spectra of XTE J1650–500 with this phenomenological but standard model. In contrast, the spectrum of GX 339–4 is robust; strong deviations consistent with a broad Fe K $\alpha$  emission line are revealed in the data/model ratio (see Figure 2).

We therefore included the “Laor” line model to the spectral model for GX 339–4. This model describes the line profile expected when an accretion disk orbiting a black hole with non-zero angular momentum ( $a = j = cJ/GM^2$ ) is irradiated by a source of hard X-rays. The line energy, inner disk emissivity index  $q$  ( $J(r) \propto r^{-q}$  where  $J(r)$  is the emissivity and  $q = 3$  is expected for a standard thin disk;  $q = 3$  was fixed to be the lower limit in all fits), the inner and outer radii of the line emitting region, the inner disk inclination, and the line normalization are free parameters. The outer emission radius was fixed to  $R_{out} = 400 R_g$  in fits with this model ( $R_g = GM/c^2$ ) and the emissivity index was constrained such that  $q \geq 3.0$ ; all other parameters were left as free parameters. The addition of this component significantly reduces the  $\chi^2$  fit statistic; the F-statistic for the inclusion of this model ( $3.6 \times 10^{-10}$ ) indicates that the Laor model is required at the  $6.3\sigma$  level of confidence. The addition of a smeared edge (“smedge” within XSPEC) is not statistically required, likely due to the low effective area of the HEG above 8 keV.

It is clear that the spectrum of XTE J1650–500 evolved significantly between the observations. In both spectra, moderate disk color temperatures are measured ( $kT = 0.610(4)$  keV and  $kT = 0.570(1)$  keV, respectively). In the first observation a moderately hard power-law ( $\Gamma = 2.5^{+0.1}_{-0.2}$ ) comprises 21% of the unabsorbed flux in the 0.5–10.0 keV band; however, in the second observation the power-law is very steep ( $\Gamma = 5.4$ ) and comprises  $< 3\%$  of the total flux. Indeed, the total flux dropped by approximately 40% between the first and second observations. The spectral parameters measured during the first observation of XTE J1650–500 indicate that the source was likely observed in the “very high” or “intermediate state”, which may only be manifestations of the same state at different source fluxes (see, e.g., Homan et al. 2001). The parameters measured in the second observation, however, indicate that XTE J1650–500 was likely observed in the “high/soft” state.

The spectral parameters measured from GX 339–4 are more like those measured in the first observation of XTE J1650–500 (the power-law is 13% of the total 0.5–10.0 keV flux in the spectrum GX 339–4). However, GX 339–4 was observed at a flux 7.4 times and 4.5 times lower than measured in the first and second observations of XTE J1650–500. Indeed, the observation of GX 339–4 was made following an extended spectrally soft state as the source transitioned to the “low/hard” state.

The *Chandra*/HETGS provides dispersive spectroscopy through the Fe K $\alpha$  line range, making it possible to learn whether an apparently broad line is intrinsically broad, comprised of a few narrow lines, or perhaps a combination of an intrinsically broad line with narrow components superimposed. This ability was exploited to show that the broad Fe K $\alpha$  emission line in Cygnus X-1 does indeed contain an intrinsically broad component likely shaped by relativistic effects (Miller et al. 2002a). Unlike Cygnus X-1, we find no narrow lines amidst

the broad line profile in GX 339–4; however the HETGS spectrum again demonstrates that the broad Fe K $\alpha$  line is intrinsically broad. The Laor line model indicates that the inner disk edge may extend as close as  $R_{in} = 2.5^{+2.0}_{-0.3} R_g$  to the black hole, which would imply black hole spin as  $R_{ISCO} = 6 R_g$  for  $a = 0$  black holes (while  $R_{ISCO} = 1.24 R_g$  for  $a = 0.998$ ). A moderate inner disk inclination is measured, consistent with prior X-ray and optical studies of GX 339–4. The line equivalent width is high ( $W_{K\alpha} = 600^{+200}_{-100}$  eV); this is broadly consistent with predictions from reflection models if the disk is highly ionized (Ross, Fabian, Young 1999). The measured line centroid energy of  $E = 6.8^{+0.2}_{-0.1}$  keV is consistent with a combination of He-like Fe XXV and H-like Fe XXVI.

The normalization of the MCD model also provides a measure of the inner disk radius:  $N = ((R_{in}/\text{km})/(d/10\text{kpc}))^2 \cos(i)$ . Assuming a distance of 4–5 kpc and an inclination of  $i = 45^\circ$ , our best-fit normalization gives  $R_{in} = 22–27$  km. Assuming  $M_{BH} = 5.8 M_\odot$  as per Hynes et al. (2003), this corresponds to  $R_{in} = 2.6–3.2 R_g$ , consistent with measurements using the Laor model. We regard the results from the Laor model as more robust, as the inner disk temperature and radius measured using the MCD model are subject to Comptonization and angle-dependent opacity distortions (Shimura & Takahara 1995; Merloni, Fabian, & Ross 2000).

We also made fits with the constant density ionized disk (“CDID”, Ross, Fabian, & Young 1999; Ballantyne, Ross, & Fabian 2001) and “pexriv” (Magdziarz & Zdziarski 1995) reflection models (see Table 1), which are more physical models describing the illumination of the accretion disk by a power-law source of hard X-rays. The CDID model is particularly well-suited to high ionization regimes, and so we used the results of fits made with the CDID model to guide our fits with pexriv (pexriv does not Comptonize absorption edges and is therefore more approximate). An important difference between these reflection models is that the CDID model explicitly includes Fe K $\alpha$  line emission, while a separate line component must be added to the total model to make proper fits with pexriv. In both cases, we convolved (or, “smeared”) the reflection model with the Laor line element to account for the strong Doppler and gravitational shifts expected near to the black hole. The reflected spectra were fit in addition to an MCD component, as a disk component is not included explicitly in either model.

Fits with the CDID model yielded a significant improvement over fits with the phenomenological model consisting of MCD, power-law, and Laor components (see Table 1). The best-fit ionization parameter is well-constrained and indicates a highly-ionized disk reflector:  $\log(\xi) = 4.0 \pm 0.4$  (where  $\xi = L_X/nr^2$  and  $n$  is the hydrogen number density). The reflection fraction is measured to be  $R = 1.2^{+2.0}_{-0.5}$  (the CDID model incorporates the  $R$  factor as:  $F_{total} = F_{incident} + R \times F_{reflected}$ ; the  $R$  parameter does not directly relate to the solid angle subtended by the disk). The ionization parameter measured is in agreement with the iron ionization state measured via the Laor model. The best-fit Laor smearing parameters ( $R_{in} = 1.3^{+1.7}_{-0.1} R_g$ ,  $q = 3.0^{+0.7}$ ,  $i = 30^\circ \pm 15^\circ$ ) again suggest a disk which extends very close to the black hole, suggesting the black hole may have a high spin parameter. In contrast to the more phenomenological model, however, the smeared CDID fits do not require a high disk emissivity index.

The results of fits made with the CDID model were used to guide fits with pexriv. We fixed the disk temperature to  $T = 1.2 \times 10^7$  K (1 keV) to correspond with the expected temperature of an ionized accretion disk skin (Young et al. 2001),

and  $\log(\xi) = 4.0$  to the above CDID result. We fit *pexriv* as a “pure” reflection spectrum (e.g., without including the power-law continuum); the irradiating power-law index and normalization were fixed to correspond to the separate power-law component. The inclination in *pexriv* was fixed to correspond to the same parameter in the relativistic smearing function. Finally, we fixed the high energy cut-off of the power law to  $E=200$  keV in view of the lack of an obvious cut-off in the 3–200 keV *RXTE* spectrum. As with the CDID model, fits with *pexriv* are statistically preferred to fits with the initial phenomenological model (see Table 1 and Figure 3). The reflection fraction (in this case,  $R \propto \Omega/2\pi$ ) is measured to be  $R = 1.0 \pm 0.4$ , indicating that the disk intercepts roughly half of the incident flux. The relativistic smearing parameter values were set to be equivalent to the parameters in the independent Laor line model. While fits with the Laor line once again indicate an ionized line ( $E = 6.92^{+0.05}_{-0.27}$  keV), the inner radius is not as well constrained from above:  $R_{in} = 1.8^{+7.0}_{-0.6} R_g$ .

### 3.2. The High Resolution Spectrum of GX 339-4

We analyzed the combined first-order MEG spectrum of GX 339-4 in narrow  $2\text{\AA}$  slices. The continuum in each slice was fit with a simple power-law model, modified by an edge due to photoelectric absorption by neutral (atomic) elements in the ISM where appropriate. Line features were fit with Gaussian models. Line identifications are based on the calculations and line lists tabulated by Verner, Verner, & Ferland (1996) and by Behar & Netzer (2002). Table 2 lists the line identifications and parameters for absorption lines detected in the spectrum of GX 339-4 (as well as XTE J1650-500, against which we later compare the spectrum of GX 339-4), as well as upper-limits for lines not clearly detected. The column density estimates were derived using the relation:

$$W_\lambda = \frac{\pi e^2}{m_e c^2} N_j \lambda^2 f_{ij} = 8.85 \times 10^{-13} N_j \lambda^2 f_{ij}$$

where  $N_j$  is the column density of a given species,  $f_{ij}$  is the oscillator strength,  $W_\lambda$  is the equivalent width of the line in cm units, and  $\lambda$  is the wavelength of the line in cm units (Spitzer 1978). We have taken all  $f_{ij}$  values for all resonant lines from Verner, Verner, & Ferland (1996) and Behar & Netzer (2002). In using this relation, we are assuming that the lines are optically thin and that we are on the linear part of the curve of growth. Fits to the spectrum of GX 339-4 are shown in Figure 4 and Figure 5.

A number of relatively strong X-ray absorption lines are clearly detected in the high resolution spectrum. We identified the observed lines using a boot-strap approach. One of the strongest lines is found at  $13.442(1)\text{\AA}$ , and we identify this line as the Ne IX He- $\alpha$  resonance line expected at  $13.447\text{\AA}$ . Absorption lines observed at  $11.541^{+0.006}_{-0.004}\text{\AA}$  and  $10.998(3)\text{\AA}$  are then very likely to be the Ne IX He- $\beta$  and He- $\gamma$  resonance lines expected at  $11.547\text{\AA}$  and  $11.000\text{\AA}$ , respectively.

With the clear identification of the He-like Ne IX resonance series, we then searched for He-like and H-like resonance absorption lines from Ne and other low-Z elements. Lines detected at  $18.964(1)\text{\AA}$  and  $16.003(4)\text{\AA}$  correspond with the O VIII Ly- $\alpha$  and Ly- $\beta$  lines expected at  $18.967\text{\AA}$  and  $16.006\text{\AA}$ , respectively. The line observed at  $18.623(1)\text{\AA}$  corresponds to the O VII He- $\beta$  line expected at  $18.627\text{\AA}$  (the He- $\alpha$  line is expected at  $21.602\text{\AA}$ , where the sensitivity of the spectrum is low).

The line detected at  $9.166^{+0.001}_{-0.002}\text{\AA}$  corresponds to the Mg XI He- $\alpha$  line expected at  $9.169\text{\AA}$ . The strongest of these highly ionized lines have velocity widths  $\leq 400$  km/s, and apparent blue-shifts of approximately 100 km/s.

The Si He-like resonance line series is not clearly detected. With the exception of O, lines from H-like series are not detected. A number of lines from the Fe L shell (especially Fe XVI and Fe XVII) are expected to be especially strong in the 12–17 $\text{\AA}$  range, but these lines are also absent in the spectrum. We measured upper limits for H-like lines and particular Fe XVI and Fe XVII lines; these upper-limits are also reported in Table 2.

Two especially strong lines are detected at  $14.606(1)\text{\AA}$  and  $14.504(2)\text{\AA}$ . These lines are not plausibly associated with any He-like or H-like lines from low-Z elements. The O VIII 1s-6p and 1s-7p transitions are expected at  $14.634\text{\AA}$  and  $14.524\text{\AA}$  (respectively), but this would imply larger blue-shifts (400–600 km/s) for these lines than for the detected O VIII 1s-2p and O VIII 1s-3p lines ( $< 100$  km/s). Moreover, the 1s-4p and 1s-5p lines are not detected, which makes any identification with O VIII very problematic. Similarly, these lines cannot plausibly be associated with Fe L-shell transitions occurring in this range, as the strongest Fe L-shell lines expected for a wide range in plasma temperature, density, and ionization parameter (see, e.g., Kallman & McCray 1982) are not detected and the upper limits are strict. In particular, although these lines are close to Fe XVIII transitions, other Fe XVIII transitions which should be stronger are not detected.

Behar and Netzer (2002) have recently calculated the 1s–2p resonance line wavelengths and oscillator strengths expected for abundant elements up to Fe. The Ne II resonance line occurs at  $14.631\text{\AA}$  and the Ne III line occurs at  $14.526\text{\AA}$ . The wavelengths calculated by Behar and Netzer (2002), if accurate, would imply blue-shifts of 400–500 km/s. If the lines at  $14.631\text{\AA}$  and  $14.526\text{\AA}$  are Ne II and Ne III resonance absorption lines, their velocity widths (500 km/s and 400 km/s, respectively) imply that the absorption may not originate in the ISM. Thermal broadening in the cool phase of the ISM is expected to be lower than 10 km/s (e.g., Vidal-Madjar et al. 1982). Such narrow lines would be highly saturated, and column densities much larger than those in Table 2 would be required to account for the measured equivalent widths. Lines similar to those we identify as Ne II and Ne III may have been detected in other sources, though not as clearly. A feature which may be a blend of the lines we have observed in GX 339-4 was found in a *Chandra*/LETGS spectrum of Cygnus X-2 and ascribed to Ne II (Takei et al. 2002). In an analysis of a *Chandra*/LETGS spectrum of 4U 0614+091 (Paerels et al. 2001), a possible absorption line was found at  $14.45\text{\AA}$ .

### 3.3. The High Resolution Spectra of XTE J1650-500

The two sensitive spectra of XTE J1650-500 obtained with the *Chandra*/HETGS provide an important background against which to contrast the results of our analysis of the GX 339-4 spectrum. Therefore, we analyzed these spectra in exactly the same manner used to analyze the spectrum of GX 339-4. Results from a preliminary analysis of the spectra of XTE J1650-500 were previously reported by Miller et al. (2002b); however, the results we report herein are based on a more refined reduction and analysis. The parameters for both detected lines and upper limits are reported in Table 2, and fits to the spectra of XTE J1650-500 are shown in Figure 6.

The Ne IX He- $\alpha$  line is not detected in the first spectrum of XTE J1650–500, and the upper limit is strict. A weak line is detected at about the  $4\sigma$  level of confidence in the second spectrum. The Mg XI He- $\alpha$  line is not detected in the spectrum from either observation, and once again the upper-limits are constraining.

The line we have identified as Ne II is detected in both spectra of XTE J1650–500, at  $14.606(3)\text{\AA}$  and  $14.609(6)\text{\AA}$  in the first and second observations, respectively. The line equivalent width (and, therefore, the implied column density) is measured to decrease slightly between the first and second observations. However, the Ne III line expected at  $14.526\text{\AA}$  and found at  $14.504(2)\text{\AA}$  in the spectrum of GX 339–4 is not clearly detected in either spectrum of XTE J1650–500. It is worth noting that the line herein identified as Ne II was originally attributed to an Fe XVIII transition in Miller et al. (2002b); for the reasons given in the previous section the prior identification is likely in error.

#### 4. DISCUSSION

##### 4.1. On the Fe K $\alpha$ Emission Line and Black Hole Spin

Fits to the Fe K $\alpha$  emission line model using the Laor line model and with the Laor-smeared CDID reflection model all point toward a scenario in which the disk may extend radially closer to the black hole than is allowed in the absence of black hole spin. The normalization of the MCD model may support these findings. The low-to-moderate inclination of GX 339–4 and relatively small contribution from the power-law act to mitigate the Comptonization and angle-dependent opacity effects which can otherwise distort inner disk temperature and radius measurements made via the MCD model.

Whereas fits to the *XMM-Newton* spectrum of XTE J1650–500 (Miller et al. 2002c) with the pexriv reflection model ruled-out  $R_{in} = 6 R_g$  at more than the  $6\sigma$  level of confidence — clearly indicating a black hole with a high spin parameter — fits to this spectrum of GX 339–4 with the same model do not rule-out  $R_{in} = 6 R_g$ . Indeed, the line profile found in this spectrum of GX 339–4 is only clearly visible above the continuum at energies above approximately 5 keV; in contrast, the line revealed in the *XMM-Newton* spectrum of XTE J1650–500 extends down to approximately 4 keV. Thus, although other fits to this spectrum and its prominent Fe K $\alpha$  emission line suggest that GX 339–4 harbors a black hole with a high spin parameter, the data must be regarded as indicative but not definitive.

Although the evidence for spin is not conclusive, this observation clearly demonstrates that long exposures can reveal the inner accretion disk in multiple and independent ways, even at relatively low fluxes. Moreover, it is also clear that even at Eddington accretion rates as low as  $\dot{m}_{Edd} \simeq 0.1 - 0.2$  (assuming  $M = 5.8 M_\odot$  and a distance of  $d = 4 - 5$  kpc), the radial extent of the inner disk in GX 339–4 is consistent with (if not less than) the ISCO for a Schwarzschild black hole. The model for Galactic black hole state transitions described by Esin, McClintock, & Narayan (1997) predicts that the inner disk edge should radially recede and be replaced by an inner ADAF just below ( $\dot{m}_{Edd} \simeq 0.08$ ) the range implied for GX 339–4 during this observation. It is worth noting that the relation between the inner disk extent and  $\dot{m}$  is unknown in these and all black hole systems (McClintock & Remillard 2003). The ADAF model does predict a recessed disk in the intermediate and low/hard states, however, and the former is likely the state in which we observed GX 339–4. Our independent findings on the inner extent of the

accretion disk are therefore in qualitative disagreement with the ADAF model for Galactic black hole state transitions. Our results are in agreement with observations which show that soft, disk-dominated states can occur at accretion rates separated by several orders of magnitude (see, e.g., Homan et al. 2001).

The reflection models we have fit to the spectrum of GX 339–4 indicate that the disk likely intercepts approximately half of the incident power-law X-ray flux (see Table 1). These results are inconsistent with models which ascribe hard X-ray production to a jet outflow (Markoff, Falcke, & Fender 2001; Markoff et al. 2003). The Lorentz factors ( $\gamma = 2 - 3$ ) required to produce hard X-ray radiation via direct synchrotron emission or synchrotron self-Comptonization necessarily beam the emission in a narrow cone along the jet axis. Assuming that the jet axis is coincident with the black hole angular momentum vector and that the inner disk is anchored in a plane perpendicular to that vector, then the degree of disk illumination indicated by fits with reflection models likely cannot be supplied by a jet source. Other work has noted that compact jet models may not be a viable explanation for the X-ray power-law component in accreting sources with a sizable disk reflection fraction (Zdziarski & Poutanen, Zdziarski et al. 2003).

##### 4.2. Evidence for a Local Warm Absorber

In an optically-thin plasma with a temperature near  $T \simeq 10^{5-6}$  K, the He-like ions of O, Ne, and Mg are expected to be important (e.g., Mazzotta et al. 1998). Some simple calculations suggest that the lines we have observed could plausibly be explained through absorption in the coronal phase of the ISM, which is at a temperature near  $10^6$  K. If we assume 1) the density of coronal gas is  $n_{coronal} = 1.0 \times 10^{-2} \text{ cm}^{-3}$ , 2) coronal gas occupies 50% of the ISM ( $f_{coronal} = 0.5$ ), 3) the abundance of Ne relative to H is  $A_{Ne} = 1.0 \times 10^{-4}$ , and 5) the distance to GX 339–4 is  $d = 4.0$  kpc, then  $N_{Ne} \simeq n_{coronal} \times f_{coronal} \times A_{Ne} \times d \simeq 6 \times 10^{15} \text{ cm}^{-2}$ . This value is rather close to that reported for GX 339–4 in Table 2. Moreover, a solar abundance plasma in collisional ionization equilibrium (Mazzotta et al. 1998) at  $T \sim 2 - 3 \times 10^6$  K comes reasonably close to matching the relative column densities of the observed ions while not violating the upper limits. Although these factors point to absorption in the ISM as a viable explanation for the observed absorption spectrum in GX 339–4 (indeed, additional deep observations of Galactic black holes are required to definitively rule-out this possibility), there are a factors which are plainly inconsistent with this explanation. Below, we discuss some difficulties with ascribing the absorption lines to the coronal ISM, and suggest that a warm absorbing geometry near to the black hole system likely provides a better explanation.

First, on examination of the He-like Ne series in the GX 339–4 spectra, the equivalent widths follow the expected ratios based on oscillator strength. This indicates that the Ne absorption lines are not saturated and retain a true shape. The width of the resolved Ne He- $\alpha$  line is  $350_{-90}^{+80} \text{ km/s}$  (FWHM), consistent with the Mg He- $\alpha$  and O Ly- $\alpha$  lines (the O line is likely partially saturated). If the lines were intrinsically narrower than 200 km/s, they would fall on the flat part of the curve of growth, giving smaller ratios between the He- $\alpha$  and He- $\beta$  lines and requiring much higher column densities. The Ne II and Ne III lines are slightly broader than even the Ne IX He- $\alpha$  line. Thermal broadening in the coronal phase of the ISM is expected to be approximately 100 km/s, which is significantly below the widths we measure from the strongest absorption lines. A local warm absorber with moderate turbulent velocity broadening

may be a better explanation for the width of the lines observed.

Second, the strongest lines in the spectrum of GX 339-4 with secure identifications have blue-shifts of approximately 100 km/s. While the absolute calibration uncertainty in the HETGS wavelength grid (0.05%) is comparable to the shifts observed, the HETGS calibration web page (<http://space.mit.edu/HETG/flight.html>) indicates that this uncertainty is likely overestimated and that shifts observed in many lines over a range in wavelength are likely reliable. If a local warm absorber in GX 339-4 is created through an accretion disk wind, then a small flow velocity into our line of sight would be expected, qualitatively consistent with the data. It is important to note that the observed shifts are not due to systemic velocities: Hynes et al. (2003) find that GX 339-4 is likely moving away at 30 km/s (Sanchez-Fernandez et al. 2002 find that XTE J1650-500 is moving away at  $19 \pm 3$  km/s).

Third, if the absorption lines in GX 339-4 are due to the coronal ISM, it is hard to reconcile the clear detection of many ionized X-ray absorption lines in GX 339-4 with the non-detection of many of the same features in XTE J1650-500. The two sources are similar in some very important ways. Both GX 339-4 and XTE J1650-500 lie within the Galactic plane:  $b_{GX\ 339-4} = -4.3$  and  $b_{1650} = -3.4$ . The equivalent neutral hydrogen density along the line of sight to these sources is also very similar:  $N_{H,GX\ 339-4} = 5.3 \times 10^{21} \text{ cm}^{-2}$  and  $N_{H,1650} = 4.9 \times 10^{21} \text{ cm}^{-2}$  (based on HI measurements in radio by Dickey & Lockman 1990). We therefore expect that the ISM should be rather similar along the line of sight to each source. Prior observations in optical and X-ray bands suggest that both systems are seen at relatively low ( $i \leq 45^\circ$ ) binary and inner disk inclinations (GX 339-4: Hynes et al. 2003, Nowak et al. 2002; XTE J1650-500: Miller et al. 2002c, Sanchez-Fernandez et al. 2002). Finally, the distances to these sources are likely similar. The *RXTE*/ASM measured a peak count-rate of 70 c/s (1.5–12 keV) during the 2002–2003 outburst of GX 339-4, and a peak count rate of 40 c/s during the 2001–2002 outburst of XTE J1650-500. Assuming that similar fractional Eddington luminosities were achieved and similar spectral shapes at peak, then the distance to these sources is not likely to differ by more than  $\sqrt{70/40} \simeq 1.3$ .

These similarities make it hard to explain how the column density of Ne IX is measured to be 30 times higher in GX 339-4 than in the first observation of XTE J1650-500, if the lines are due to absorption in the coronal ISM. The source distances certainly do not differ by a factor of 30. It is also very unlikely that the distance and abundance of Ne IX in the ISM both differ by  $\sqrt{30}$ . Moreover, the column density of Ne IX is measured to increase significantly between the first observation (made at a flux of 0.4 Crab) and the second observation (made at a flux of 0.25 Crab) of XTE J1650-500 (the column density in the second observation is 2.3 times higher than the upper-limit in the first observation). Note that the observation of GX 339-4 – wherein Ne IX is clearly detected – occurred at a flux below 0.1 Crab.

In view of these difficulties, a warm absorber (see, e.g., Reynolds 1997) local to GX 339-4 that is created by a disk wind or a shell ejection event seems to provide a much better explanation for the discrepant and changing line fluxes than absorption within the ISM. Alternatively, the disk may not contribute a substantial outflow, but the ionization of an absorber may fall as the central source flux decays, allowing lines to be observed as the outburst decays. Thus, we are left with two

possibilities: either the line of sight to GX 339-4 is special, for instance passing through a supernova remnant, or else the absorbing gas is photoionized circumstellar material. At the time of writing, we have found no published claims for a supernova remnant along this line of sight. There is evidence for an outflowing absorber in XTE J1650-500 as well; however, we have chosen to focus this discussion and modeling efforts on GX 339-4 as the evidence is much stronger.

#### 4.3. Photoionized Plasma Models

X-ray absorption lines have been detected in Galactic black holes with low-mass donors observed with ASCA (GRO J1655-40: Ueda et al. 1998, GRS 1915+105: Kotani et al. 2000). In contrast to GX 339-4 and XTE J1650-500, these sources are viewed at high inclinations, and the observed lines are consistent with Fe XXV and Fe XXVI. The absorbing geometry in these sources is very likely the hot Comptonizing corona thought to contribute to hard power-law emission, or an ionized skin above the accretion disk. If the lines in the relatively face-on GX 339-4 and XTE J1650-500 are due to local warm absorbers, the absorber is likely of a different nature. Certainly, the fact that only lines from low-Z elements are observed signals an absorber which is likely 10–100 times colder than a standard corona.

The warm absorber required might be analogous to those seen in some Seyfert galaxies, perhaps fed through a disk-driven outflow (Elvis 2000, Morales & Fabian 2002, Turner et al. 2003). In contrast to a recent model for AGN spectra which relies on an optically-thick outflow (King & Pounds 2003); it is clear that any disk-driven outflow in GX 339-4 and XTE J1650-500 must be *optically thin*. First, the spectra are well-described by an optically thin gas in photoionization equilibrium. Second, the inner disk is revealed through the hot disk component and relativistic Fe K $\alpha$  line, both of which would be obscured by an optically thick outflow.

To further investigate this idea we have computed the equivalent widths of the observed absorption lines using the atomic physics packages described in Raymond (1993). Briefly, these include heating by photoionization and Compton scattering and cooling by line and continuum emission and Compton scattering. The predicted ionization state is combined with a curve of growth (Spitzer 1978) for a chosen velocity width to determine the equivalent widths.

We specify the ionizing spectrum using the blackbody and power-law parameters in Table 1. Placing a  $10^7$  cm thick slab with a density of  $3 \times 10^{13} \text{ cm}^{-3}$  at a distance of  $2 \times 10^{11}$  cm from the X-ray source gives an ionization parameter  $\xi = L/nr^2$  of 70. It predicts about the right Ne IX equivalent widths for a 250 km/s line width as well as reasonable values for the Ne X, Mg XI and Fe XVII lines (see Table 2 and Table 3), but it over-predicts the oxygen equivalent widths assuming solar abundances (including the Allende-Prieto, Lambert & Asplund (2001) value for oxygen). A narrower width would saturate the oxygen lines and reduce their equivalent widths, but predict incorrect line ratios. In reality it is likely that the actual absorption profiles are complex mixtures of wide and narrow features, some of which are saturated and some not. See Table 3 for a list of the equivalent widths predicted by the model as a function of velocity width.

Any slab having the the same ionization parameter ( $n \propto r^{-2}$ ) and appropriate thickness ( $\delta r \propto r^2$ ) would give the same equivalent widths. The posited slab is very thin compared to its distance from the central source if it is located in system it-

self, that is a distance of a few solar radii. It might be an intrinsically-thin structure, such as an accretion stream, or it could actually correspond to dense clumps in a wind that is otherwise so low in density and therefore so high in ionization state that it contains no ions detectable in our wavelength range. Such explanations appear more likely when the mass outflow rate is considered. The mass outflow rate can be estimated via  $\dot{m}_{out} \sim 4\pi f L_X m_p v \xi^{-1}$  (where  $f$  is the filling factor,  $m_p$  is the proton mass,  $v \sim 100$  km/s is the outflow velocity, and  $\xi \sim 70$  is again the ionization parameter), and  $\dot{m}_{out} \sim f \times 5 \times 10^{-7} M_\odot/\text{yr}$ . However, we expect the time averaged mass inflow rate to be approximately  $\dot{m} \sim 10^{-9} M_\odot/\text{yr}$  (Frank, King, & Raine 2002). In order not to exceed the expected inflow rate (at least, for long periods), a shell ejection may be required to explain the data. Alternatively,  $f$  may be quite small, consistent with a clumpy absorbing geometry or a sheet-like wind outflow that has a small filling factor. The warm absorber geometry in Seyfert 1 galaxies may not be homogeneous, but in fact comprised of clouds which are radiatively driven from the central accretion engine. Indeed, mass upper limits derived assuming radiatively-driven absorbing clouds are very similar to estimates derived via reverberation mapping and velocity dispersion laws for a number of Seyfert 1 galaxies (Morales and Fabian 2002). Elvis (2000) has described a model for AGN in which winds flow from the disk in a sheet-like geometry.

## 5. SUMMARY AND CONCLUSIONS

We have analyzed the broad-band and high-resolution X-ray spectrum of the Galactic black hole GX 339–4 during outburst decline. The spectral resolution of the *Chandra*/HETGS and the high sensitivity achieved during our long 75 ksec observations have permitted a number of important findings.

First, the broad Fe  $K\alpha$  line previously observed in GX 339–4 (e.g., Nowak et al. 2002) is indeed *intrinsically* broad and skewed, indicating that it is likely shaped by relativistic effects at the inner edge of an accretion disk. Fits with relativistic line models and relativistically-smearing reflection models suggest that the black hole in GX 339–4 may have significant angular momentum.

Second, we have clearly detected X-ray absorption lines from He-like and H-like O, and He-like Ne and Mg. This is the first time that highly ionized X-ray absorption lines from elements with  $Z < 20$  have been observed in a dynamically-constrained Galactic black hole system with a low-mass donor star. These absorption lines may be due to absorption in the coronal ISM,

but are far more likely to be due to a photoionized warm absorber local to the system. The observed blue-shift of the absorption lines indicate the absorbing material may be outflowing from the system. Models describing a warm absorber with a modest ionization parameter ( $\xi = 70$ ) and velocity width (150–250 km/s), and illuminated by a combination of black-body and power-law fluxes of the magnitude we have measured in GX 339–4, can approximate the observed absorption spectrum. The absorber may have resulted from a disk-driven outflow, may be clumpy, and qualitatively similar to the warm absorber geometries inferred in Seyfert 1 galaxies.

Thirdly, and most importantly, this observation has likely established another important link between stellar-mass Galactic black holes and supermassive black holes in AGN. It has become clear that skewed, relativistic Fe  $K\alpha$  lines imply that the inner accretion flow geometry in some Galactic black hole states may be very similar to that in Seyfert 1 galaxies (Wilms et al. 2001, Miller et al. 2002a, Miller et al. 2002c). The detection of large-scale relativistic jets in X-rays in XTE J1550–564 (Corbel et al. 2002) may provide a window into large-scale jet formation in some AGN. This observation indicates that X-ray warm absorbers — plausibly produced via a disk wind — may be common to both stellar mass black holes and Seyfert galaxies. The long dynamical timescales in AGN make it difficult to observe changes in the warm absorber and to clearly link effects to the central accretion engine. Future sensitive observations of Galactic black holes may reveal that stellar-mass black holes are accessible laboratories for studying the nature of X-ray warm absorbers.

## 6. ACKNOWLEDGMENTS

We wish to thank CXC Director Harvey Tananbaum and the CXC staff for granting this DDT observation. JMM thanks the University of Cambridge Institute of Astronomy for its hospitality, and Roderick Joshnstone for great computing support. We wish to thank Danny Steeghs, Adrian Turner, Anil Pradhan, Randall Smith, and Norbert Schulz for useful discussions, and John Houck for assistance with ISIS. JMM gratefully acknowledges support from the NSF through its Astronomy and Astrophysics Postdoctoral Fellowship program. JAT acknowledges partial support from NASA grant NAG5–13055. WHGL gratefully acknowledges support from NASA. This research has made use of the data and resources obtained through the HEASARC on-line service, provided by NASA-GSFC.

## REFERENCES

- Allende-Pietro, C., Lambert, D. L., & Asplund, M., 2001, *ApJ*, 556, L63  
 Arnaud, K. A., and Dorman, B., 2000, XSPEC is available via the HEASARC on-line service, provided by NASA/GSFC  
 Ballantyne, D. R., Ross, R. R., & Fabian, A. C., 2001, *MNRAS*, 323, 506  
 Behar, E., and Netzer, H., 2002, *ApJ*, 570, 165  
 Belloni, T., Mendez, M., van der Klis, M., Lewin, W. H. G., & Dieters, S., 1999, *ApJ*, 519, 159  
 Brandt, W. N., and Schulz, N. S., 2000, *ApJ*, 544, L123  
 Corbel, S., Fender, R. P., Tzioumis, A. K., Tomsick, J. A., Orosz, J. A., Miller, J. M., Wijnands, R., & Kaaret, P., 2002, *Science*, 298, 196  
 Dickey, J. M., and Lockman, F. J., 1990, *ARA&A*, 28, 215  
 Elvis, M., 2000, *ApJ*, 545, 63  
 Esin, A. A., McClintock, J. E., & Narayan, R., 1997, *ApJ*, 489, 865  
 Fabian, A. C., Guilbert, P. W., Motch, C., Ricketts, M., Ilovaisky, S. A., & Chevalier, C., 1982, *A&A*, 111, L9  
 Fender, R. P., et al. 1999, *ApJ*, 519, L165  
 Frank, J., King, A. R., & Raine, D., 2002, “Accretion Power in Astrophysics”, 3rd edition, Cambridge: Cambridge Univ. Press  
 Grebenev, S. A., Sunyaev, R., Pavlinsky, M. N., & Dekhanov, I. A., 1991, *SAL*, 1991, 17, 413  
 Homan, J., Wijnands, R., van der Klis, M., Belloni, T., van Paradijs, J., Klein-Wolt, M., Fender, R., & Mendez, M., 2001, *ApJS*, 132, 377  
 Houck, J. C., & Denicola, L. A., 2000, *Astronomical Data Analysis Software and Systems IX*, in ASP Conference Proceedings, vol. 216, eds. N. Manset, C. Veillet, & D. Crabtree; ISIS is available at <http://space.mit.edu/CXC/ISIS>  
 Hynes, R. I., Steeghs, D., Casares, J., Charles, P. A., & O’Brien, K., 2003, *ApJ*, 583, L95  
 Ilovaisky, S. A., Chevalier, C., Motch, C., and Chiapetti, L., 1986, *A&A*, 164, 671  
 Imamura, J. N., Kristian, J., Middleditch, J., and Steiman-Cameron, T. Y., 1990, 365, 312  
 Kallman, T. R., and McCray, R., 1982, *ApJS*, 50, 263  
 King, A. R., and Pounds, K. A., 2003, *MNRAS*, in press  
 Kong, A. H., Charles, P. A., Kuulkers, E., and Kitamoto, S., 2002, *MNRAS*, 329, 588  
 Kotani, T., Ebisawa, K., Dotani, T., Inoue, H., Nagase, F., Tanaka, Y., & Ueda, Y., 2000, *ApJ*, 539, 413  
 Laor, A., 1991, *ApJ*, 376, 90  
 Magdziarz, P., and Zdziarski, A. A., 1995, *MNRAS*, 273, 837  
 Markoff, S., Falcke, H., & Fender, R., 2001, *A&A*, 372, L25

- Mazzotta, P., Mazzitelli, G., Colafrancesco, S., & Vittorio, N., 1998, *A&AS*, 133, 403
- Markoff, S., Nowak, M., Corbel, S., Fender, R., & Falcke, H., 2003, *A&A*, 397, 645
- McClintock, J. E., and Remillard, R. A., 2003, astro-ph/0306213, to appear in “Compact Stellar X-ray Sources”, Cambridge University Press, eds. W. H. G. Lewin and M. van der Klis
- Mendez, M., and van der Klis, M., 1997, *ApJ*, 479, 926
- Merloni, A., Fabian, A. C., & Ross, R. R., 2000, *MNRAS*, 313, 193
- Miller, J. M., et al. 2002a, *ApJ*, 578, 348
- Miller, J. M., et al. 2002b, *ATEL* 81
- Miller, J. M., et al. 2002c, *ApJ*, 560, L69
- Miyamoto, S., Kimura, K., Kitamoto, S., Dotani, T., & Ebisawa, K., 1991, *ApJ*, 383, 784
- Miyamoto, S., Iga, S., Kitamoto, S., & Kamodo, Y., 1993, *ApJ*, 403, L39
- Miyamoto, S., Kitamoto, S., Hayashida, K., Egoshi, W., 1995, *ApJ*, 442, L13
- Morales, R., and Fabian, A. C., 2002, *MNRAS*, 329, 209
- Motch, C., Ricketts, M. J., Page, C. G., Ilievsky, S. A., & Chevalier, C., 1983, *A&A*, 119, 171
- Nowak, M. A., Wilms, J., & Dove, J. B., 2002, *MNRAS*, 332, 856
- Paerels, F., et al. 2001, *ApJ*, 546, 338
- Poutanen, J., & Zdziarski, A. A., 2002, *Proc. of the 4th Microquasar Workshop*, eds. Ph. Durouchoux, Y. Fuchs, & J. Rodriguez, published by the Center for Space Physics: Kokata
- Raymond, J. C., 1993, *ApJ*, 412, 267
- Reynolds, C. S., 1997, *MNRAS*, 286, 513
- Ross, R. R., Fabian, A. C., & Young, A. J., 1999, *MNRAS*, 306, 461
- Sanchez-Fernandez, C., Zurita, C., Casares, J., Castro-Tirado, A. J., Bond, I., Brandt, S., & Lund, N., 2002, *IAU Circ.* 7989
- Shimura, T., and Takahara, F., 1995, *ApJ*, 445, 780
- Spitzer, L., 1978, in “Physical Processes in the Interstellar Medium”, Wiley-Interscience, New York
- Steiman-Cameron, T. Y., Imamura, J. N., Middleditch, J., & Kristian, J., 1990, *ApJ*, 359, 197
- Takei, Y., Fujimoto, R., Mitsuda, K., & Onaka, T., 2002, *ApJ*, 581, 307
- Turner, A. K., Fabian, A. C., Vaughan, S., & Lee, J. C., 2003, *MNRAS*, subm., astro-ph/0303418
- Ueda, Y., Inoue, H., Tanaka, Y., Ebisawa, K., Nagase, F., Kotani, T., & Gehrels, N., 1998, *ApJ*, 492, 782
- Verner, D. A., Ferland, G. J., Korista, K. T., & Yakovlev, D. G., 1996, *ApJ*, 465, 487
- Vidal-Madjar, A., Firlet, R., Laurent, C., & York, D. G., 1982, *ApJ*, 260, 128
- Wilms, J., Nowak, M., Dove, J. B., Fender, R. P., & di Matteo, T., 1999, *ApJ*, 522, 460
- Wilms, J., Reynolds, C. S., Begelman, M. C., Reeves, J., Molendi, S., Staubert, R., & Kendziorra, E., 2001, *MNRAS*, 328, L27
- Young, A. J., Fabian, A. C., Ross, R. R., & Takanak, Y., 2001, *MNRAS*, 305, 1045
- Zdziarski, A. A., Lubinski, P., Gilfanov, M., & Revnitsev, M., 2003, *MNRAS*, 342, 355



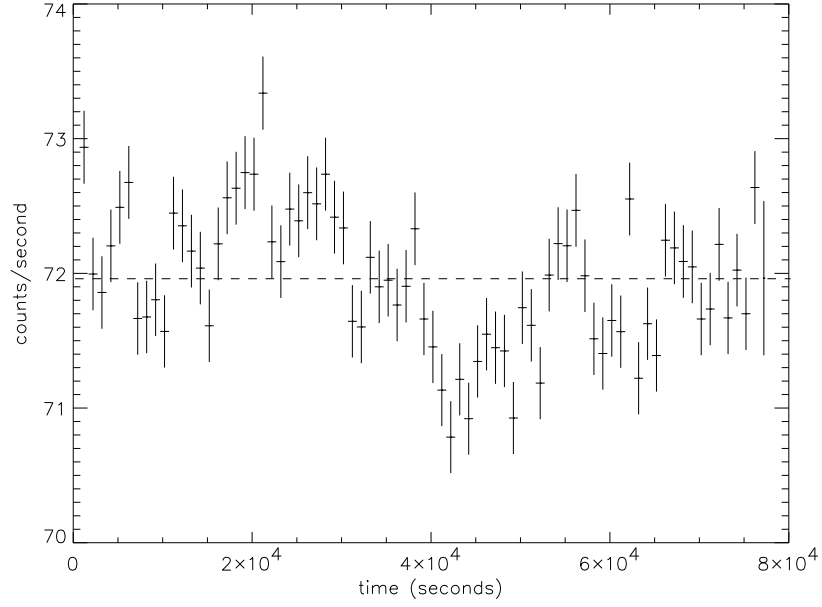


FIG. 1.— *Chandra* observed GX 339-4 for approximately 75 ksec starting on 2003 March 17.8 as it transitioned to the low/hard state. The 0.3–10.0 keV dispersed counts lightcurve is shown above (each time bin is 1000 seconds). The dashed horizontal line indicates the mean count rate. The flux is very steady over the course of the observation; variations are less than 2% of the mean.

TABLE 1

Models for the 1.2–10.0 keV Spectrum of GX 339–4 and XTE J1650–500

Observation	GX 339–4 (simple model)	GX 339–4 (pexriv <sup>a</sup> )	GX 339–4 (CDID <sup>b</sup> )	XTE J1650–500 A (simple model) <sup>c</sup>	XTE J1650–500 B (simple model) <sup>c</sup>
$N_H$ ( $10^{21}$ cm <sup>-2</sup> )	3.9(1)	4.3(1)	4.3(2)	5.6(2)	5.3(1)
<b>MCD</b>					
$kT$ (keV)	0.569(4)	0.56(1)	0.56(1)	0.610(4)	0.570(1)
Norm. ( $10^3$ )	2.04(5)	2.13(5)	2.21(5)	10.3(2)	10.6(2)
<b>power-law</b>					
$\Gamma$	2.5(1)	2.70 <sup>+0.1</sup> <sub>-0.1</sub>	–	2.5 <sup>+0.1</sup> <sub>-0.2</sub>	5.4
Norm.	0.15(2)	0.18(6)	–	1.8 <sup>+0.3</sup> <sub>-0.6</sub>	< 0.1
<b>Laor/smearing</b>					
$E$ (keV)	6.8(2)	6.92 <sup>+0.05</sup> <sub>-0.27</sub>	–	–	–
$R_{in}$ ( $R_g$ )	2.5 <sup>+2.0</sup> <sub>-0.3</sub>	1.8 <sup>+7.0</sup> <sub>-0.6</sub>	1.3 <sup>+1.7</sup> <sub>-0.1</sub>	–	–
$q$	4.5(6)	3.0 <sup>+0.6</sup> <sub>-0.2</sub>	3.0 <sup>+0.7</sup> <sub>-0.1</sub>	–	–
$i$	40(20)	15 <sup>+15</sup>	30(15)	–	–
Norm. ( $10^{-3}$ )	1.8 <sup>+0.5</sup> <sub>-0.3</sub>	1.0(4)	–	–	–
$EW$ (eV)	600 <sup>+300</sup> <sub>-100</sub>	860 <sup>+340</sup> <sub>-340</sub>	–	–	–
<b>reflection</b>					
$\Gamma$	–	–	2.6(1)	–	–
$R$	–	1.0(4)	1.2 <sup>+0</sup> <sub>-0.5</sub>	–	–
$E_{cut}$ (keV)	–	200	–	–	–
$T_{disk}$ ( $10^7$ K)	–	1.2	–	–	–
$\log(\xi)$ ( $10^4$ )	–	4.0	4.0(4)	–	–
Norm.	–	–	$7(3) \times 10^{-27}$	–	–
$\chi^2/\nu$	4116.2/3625 <sup>†</sup>	4029.0/3619	4069.9/3619	4411.8/3631	4656.3/3629
$f_{hard,0.5-10}$	0.13	0.20	0.26	0.21	< 0.03
$F_{0.5-10}$ ( $10^{-8}$ cgs)	0.42(2)	0.45(2)	0.48(2)	3.1(1)	1.9(1)
$L_{0.5-10}$ ( $10^{37}$ erg/s, $d = 4$ kpc)	0.80(4)	0.86(4)	0.9(4)	5.9(2)	3.6(1)
$L_{0.5-10}$ ( $10^{37}$ erg/s, $d = 5$ kpc)	1.26(6)	1.35(6)	1.44(6)	9.3(3)	5.7(2)

NOTE.—The results of fits to the combined first-order spectra of GX 339–4 and XTE J1650–500 in the 1.2–10.0 keV band are listed above. Errors are 90% confidence errors. Where errors are not quoted, the parameter was fixed at the value reported. The power-law indices were constrained to be within  $\Delta\Gamma \leq 0.2$  of the value measured with *RXTE* in the 3–200 keV band. An “inverse” edge component ( $E=2.07$  keV,  $\tau=-0.13$ ) was included in all models to account for the well-known instrumental Ir edge. The fluxes quoted above are “unabsorbed” fluxes. The fits obtained are not formally acceptable; the poor reduced  $\chi^2$  values very likely reflect calibration problems (such as the Ir edge) rather than any deficiency with the models used.

<sup>a</sup> The reflection model was “smeared” or convolved with the Laor line element, with all parameters of the smearing function and separate Laor line component itself constrained to be equivalent. The power-law index and normalization within the smeared “pure” reflection component were fixed to those of the external power-law.

<sup>b</sup> the reflection model was “smeared” with the Laor line component; the reflection model includes line emission explicitly.

<sup>c</sup> We have only fit simple models to XTE J1650–500; the position of chip edges due to the chosen Y offset complicates detection of broad Fe  $K\alpha$  lines revealed in simultaneous *RXTE* data.

<sup>†</sup> The best fit model without the Laor component gives  $\chi^2/\nu = 4176.5/3630$ , or an F-statistic of  $3.6 \times 10^{-10}$ , signaling this component is required at the  $6.3\sigma$  level of confidence.

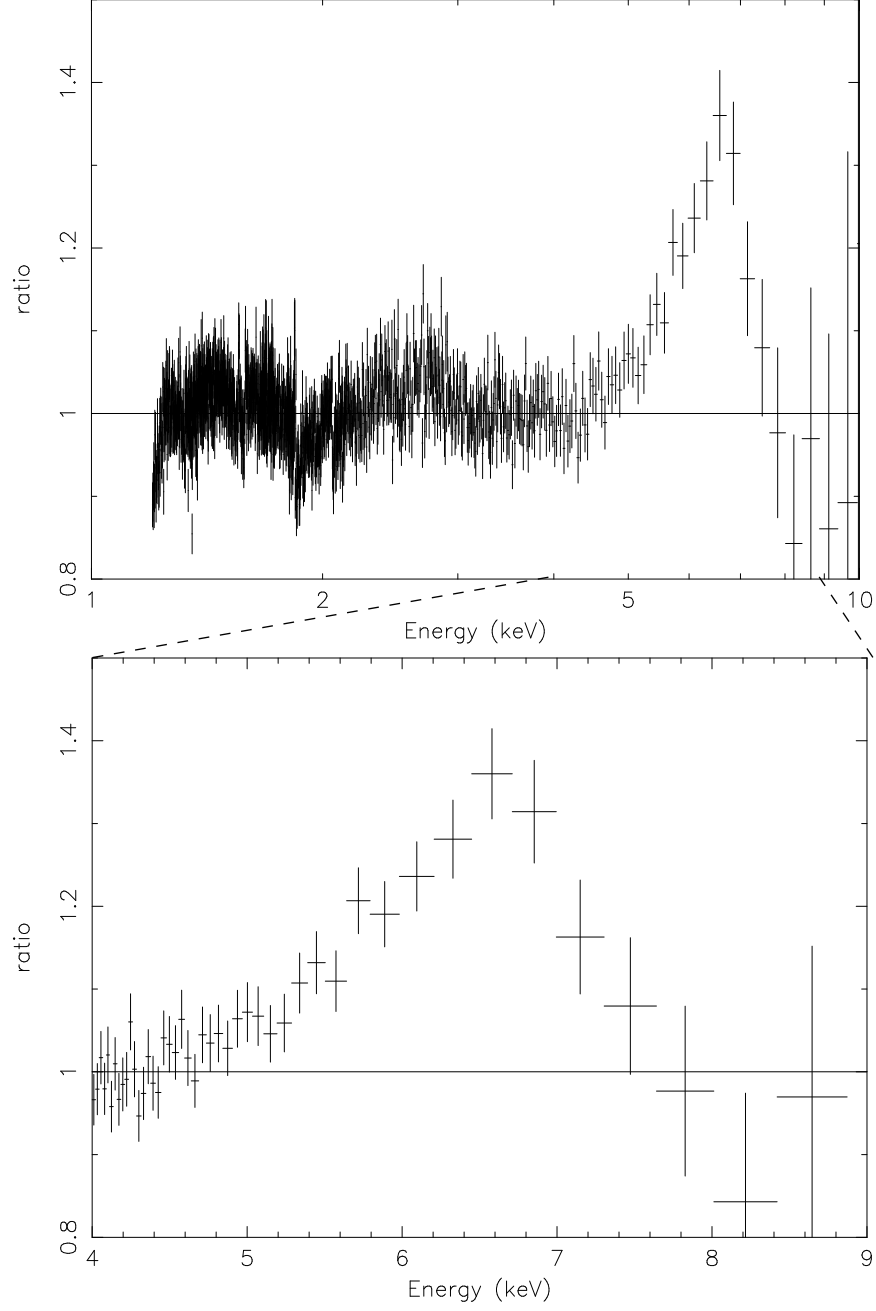


FIG. 2.— The data/model ratio obtained when the time-averaged combined first-order HEG spectra from GX 339–4 are fit with an MCD plus power-law model, assuming  $\Gamma = 2.5$  (as per fits to simultaneous *RXTE* observations on the 3.0–100.0 keV band). The 4.0–7.0 keV line region was ignored in fitting the model, and the data have been rebinned for visual clarity. An asymmetric Fe  $K\alpha$  emission line is clearly revealed. The broad line profile signals that the disk extends close to the black hole even at the mass accretion rate ( $\dot{m}_{Edd} \simeq 0.1$ ) inferred from this observation.

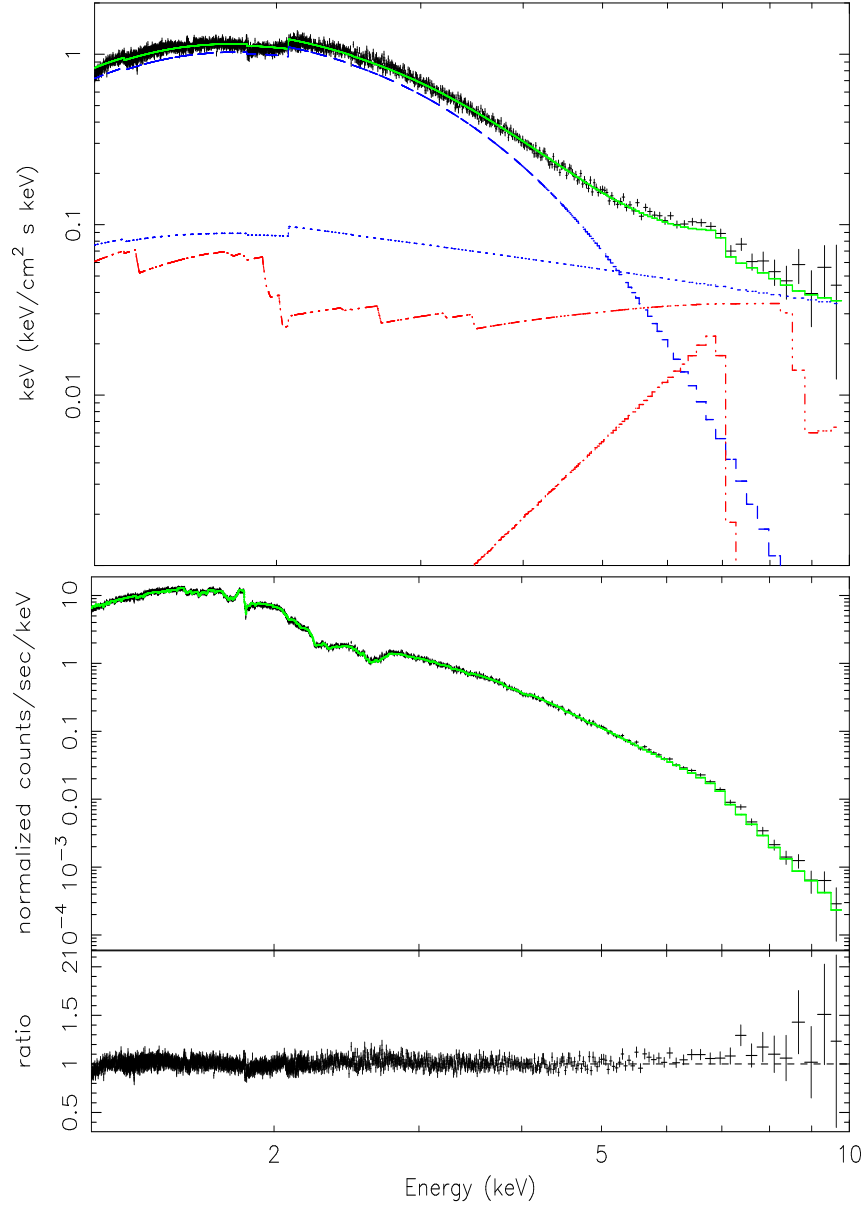


FIG. 3.— The combined first-order HEG spectra of GX 339-4 fit with a relativistically-smeared reflection model (“pexriv”, see Table 1) in the 1.2–10.0 keV band. The plot above shows the “unfolded” spectrum and components within the model. The total model is shown in green, the MCD and power-law continuum are shown in blue, and the reflection model and Laor Fe  $K\alpha$  emission line component are shown in red. Below, the count spectrum and data/model ratio are shown, with the model again shown in green. In both plots, the spectrum has been rebinned for visual clarity.

TABLE 2

Absorption Lines and Line Flux Limits in GX 339-4 and XTE J1650-500

Ion and Transition	Theor. (Å)	Meas. (Å)	Shift (km/s)	FWHM (10 <sup>-3</sup> Å)	W (km/s)	W (mÅ)	Flux (10 <sup>-4</sup> ph/cm <sup>2</sup> /s)	N <sub>Z</sub> (10 <sup>16</sup> cm <sup>-2</sup> )
— GX 339-4 —								
O VIII 1s-2p	18.967	18.964(1)	50 <sup>+20</sup> <sub>-20</sub>	23 <sup>+11</sup> <sub>-9</sub>	370 <sup>+170</sup> <sub>-350</sub>	-19(5)	-0.8(2)	1.5(4)
O VII 1s <sup>2</sup> -1s3p	18.627	18.623(1)	60 <sup>+10</sup> <sub>-10</sub>	9 <sup>+18</sup> <sub>-9</sub>	140 <sup>+280</sup> <sub>-140</sub>	-14 <sup>-5</sup> <sub>+3</sub>	-0.7(2)	3.2 <sup>+1.0</sup> <sub>-0.7</sub>
O VIII 1s-3p	16.006	16.003(4)	60 <sup>+70</sup> <sub>-80</sub>	23 <sup>+19</sup> <sub>-23</sub>	430 <sup>+360</sup> <sub>-430</sub>	-5(2)	-0.6 <sup>-0.3</sup> <sub>+0.2</sub>	3(1)
Ne II	14.631	14.606(1)	510(20)	20 <sup>+6</sup> <sub>-5</sub>	400 <sup>+130</sup> <sub>-100</sub>	-13(1)	-2.7(3)	11(1)
Ne III	14.526	14.504(2)	450(40)	24 <sup>+3</sup> <sub>-5</sub>	500 <sup>+80</sup> <sub>-100</sub>	-11(1)	-2.4(3)	5.7(7)
Ne IX 1s <sup>2</sup> -1s2p	13.447	13.442(1)	110 <sup>+30</sup> <sub>-20</sub>	16(4)	350 <sup>+80</sup> <sub>-90</sub>	-17(1)	-3.8(3)	1.4(1)
Ne IX 1s <sup>2</sup> -1s3p	11.547	11.541 <sup>+0.004</sup> <sub>-0.001</sub>	160 <sup>+20</sup> <sub>-100</sub>	3.0 <sup>+10</sup> <sub>-3</sub>	80 <sup>+250</sup> <sub>-80</sub>	-3(1)	-1.2(1)	1.7(6)
Ne IX 1s <sup>2</sup> -1s4p	11.000	10.998(3)	60 <sup>+80</sup> <sub>-90</sub>	2.4 <sup>+8.2</sup> <sub>-2.4</sub>	70 <sup>+40</sup> <sub>-70</sub>	-1.6 <sup>-0.2</sup> <sub>+0.4</sub>	-0.8 <sup>-0.1</sup> <sub>+0.2</sub>	2.0 <sup>+0.5</sup> <sub>-0.3</sub>
Mg XI 1s <sup>2</sup> -1s2p	9.169	9.166 <sup>+0.001</sup> <sub>-0.002</sub>	100 <sup>+60</sup> <sub>-30</sub>	10 <sup>+5</sup> <sub>-8</sub>	330 <sup>+170</sup> <sub>-250</sub>	-2.4 <sup>-0.2</sup> <sub>+0.1</sub>	-1.5 <sup>-0.1</sup> <sub>+0.2</sub>	0.45 <sup>+0.03</sup> <sub>-0.02</sub>
O VII 1s <sup>2</sup> -1s4p	17.768	—	—	24	400	-6 <sup>-3</sup> <sub>+3</sub>	-0.4(2)	4(2)
O VIII 1s-4p	15.176	—	—	20	400	-2.2 <sup>-0.5</sup> <sub>+1.0</sub>	-0.4 <sup>-0.1</sup> <sub>+0.2</sub>	4 <sup>+1</sup> <sub>-2</sub>
Fe XVI	16.63	—	—	22	400	-1 <sup>-2</sup> <sub>+1</sub>	-0.1 <sup>-0.2</sup> <sub>+0.1</sub>	—
Fe XVII	15.015	—	—	20	400	-1.6 <sup>-1.6</sup> <sub>+1.0</sub>	-0.3 <sup>-0.3</sup> <sub>+0.2</sub>	0.03 <sup>+0.03</sup> <sub>-0.02</sub>
Fe XVII	13.823	—	—	18	400	-0.7 <sup>-0.3</sup> <sub>+0.7</sub>	-0.2 <sup>-0.3</sup> <sub>+0.2</sub>	0.10 <sup>+0.15</sup> <sub>-0.10</sub>
Ne X 1s-2p	12.1339	—	—	16	400	-0.6(6)	-0.2(2)	0.1(1)
Fe XVII	12.120	—	—	16	400	-0.6 <sup>-0.9</sup> <sub>+0.6</sub>	-0.2 <sup>-0.3</sup> <sub>+0.2</sub>	0.06 <sup>+0.09</sup> <sub>-0.06</sub>
Mg XII 1s-2p	8.421	—	—	11	400	-0.06(6)	-0.04(4)	0.03(3)
Si XII 1s <sup>2</sup> -1s2p	6.648	—	—	8.5	400	-9(5)	-0.6(3)	0.3(2)
Si XIV 1s-2p	6.61822	—	—	8	400	-0.4(4)	-0.3(3)	0.3(3)
— XTE J1650-500 Observation A —								
Ne II	14.631	14.606(3)	510(60)	26 <sup>+8</sup> <sub>-7</sub>	530 <sup>+160</sup> <sub>-140</sub>	-8(1)	-9(2)	7(1)
Ne III	14.526	—	—	—	—	-4(1)	-4(1)	2.0(6)
Ne IX 1s <sup>2</sup> -1s2p	13.447	—	—	—	—	-0.7 <sup>-1.1</sup> <sub>+0.7</sub>	-0.8 <sup>-1.4</sup> <sub>+0.8</sub>	0.06 <sup>+0.09</sup> <sub>-0.06</sub>
Mg XI 1s <sup>2</sup> -1s2p	9.169	—	—	—	—	-0.5 <sup>-0.3</sup> <sub>+0.5</sub>	-2 <sup>-1</sup> <sub>+2</sub>	0.09 <sup>+0.05</sup> <sub>-0.09</sub>
— XTE J1650-500 Observation B —								
Ne II	14.631	14.609(6)	450(90)	12 <sup>+8</sup> <sub>-12</sub>	240 <sup>+160</sup> <sub>-240</sub>	-6(1)	-4.7(8)	5.2(9)
Ne III	14.526	14.510(5)	—	2.4 <sup>+2.4</sup> <sub>-2.4</sub>	50 <sup>+50</sup> <sub>-50</sub>	-2.6(8)	-2.1(7)	1.4(5)
Ne IX 1s <sup>2</sup> -1s2p	13.447	13.450(3)	-70 <sup>-60</sup> <sub>+70</sub>	16(4)	2.4 <sup>+2.4</sup> <sub>-2.4</sub>	-3.9(9)	-3.5(8)	0.34(8)
Mg XI 1s <sup>2</sup> -1s2p	9.169	—	—	—	—	-0.7 <sup>-2.5</sup> <sub>+0.7</sub>	-0.2 <sup>-0.7</sup> <sub>+0.2</sub>	0.1 <sup>+0.5</sup> <sub>-0.1</sub>

NOTE.—Absorption lines found in the *Chandra*/HETGS MEG spectra of GX 339-4 and XTE J1650-500. The continua were fit locally using power-law models modified by neutral photoelectric absorption edges (due to the ISM) where appropriate. The lines were fit with simple Gaussian models (see Figures 4, 5, and 6). The errors quoted above are 1 $\sigma$  uncertainties. Line widths consistent with zero are not unresolved. For GX 339-4, we have included upper-limits on important lines, as these limits which may enable others to readily develop models for the nature of the absorber. Where an XTE J1650-500 line wavelength measurement is not given, the line parameters are upper-limits assuming the same FWHM and centroid wavelength as the corresponding GX 339-4 line. Line wavelengths and oscillator strengths are taken from Verner, Verner, and Ferland (1996), except parameters for Ne II and Ne III which are taken from Behar and Netzer (2002).

TABLE 3

Photoionized Plasma Models for GX 339-4: Equivalent Width As a Function of Velocity Width

Ion & Wavelength (Å)	EW (Meas., mÅ)	EW (mÅ)	EW (mÅ)	EW (mÅ)	EW (mÅ)	EW (mÅ)	EW (mÅ)
		50 km/s	150 km/s	250 km/s	350 km/s	450 km/s	550 km/s
O VIII 18.967Å	19.0	11.63	28.58	41.36	50.85	57.32	64.51
O VII 18.627Å	14.0	7.38	12.24	13.84	14.64	15.12	15.45
O VIII 16.006Å	5.0	6.41	10.65	12.06	12.77	13.20	13.51
Ne IX 13.447Å	17.0	5.86	10.36	12.05	12.88	13.44	13.79
Ne IXb 11.547Å	3.0	1.88	2.18	2.25	2.30	2.30	2.30
Ne X 12.13Å	< 3.0	3.00	3.85	4.06	4.15	4.21	4.26
Mg XI 9.166Å	2.4	1.39	1.60	1.64	1.67	1.67	1.67
Fe XVII 15.010Å	< 3.0	5.03	7.38	8.08	8.43	8.59	8.72
Fe XVIII 14.610Å	< 10.0	0.31	0.31	0.31	0.31	0.31	0.31

NOTE.—Absorption line equivalent widths as a function of velocity width for a photoionized absorption models based on the code of Raymond (1993); see Section 4.3 for details. The models above were generated assuming solar elemental abundances. A velocity width of 150 km/s is likely the best match to the absorption lines observed in GX 339-4; abundances differing slightly from solar values may be required to explain the observed Mg/O and Ne/O ratios.

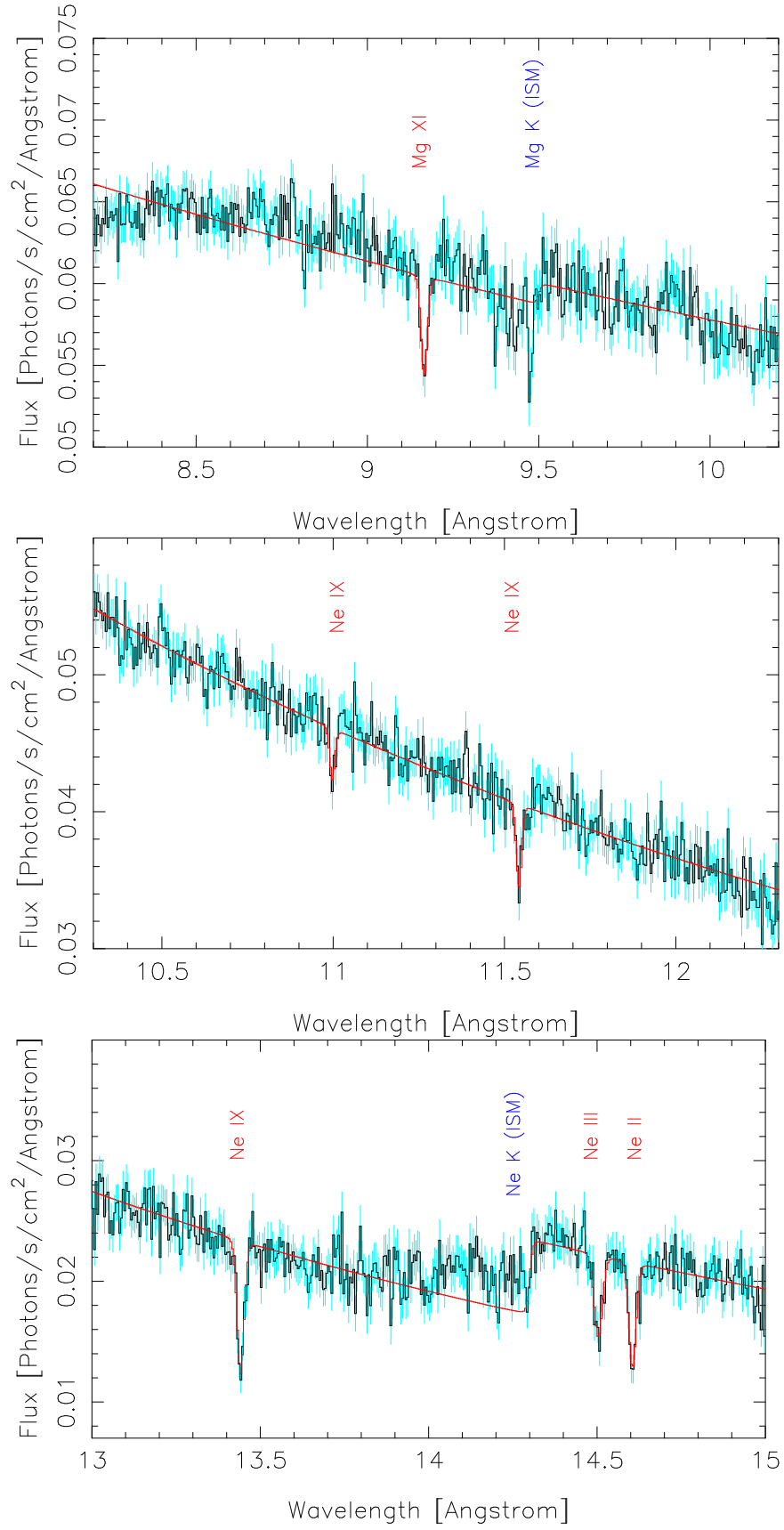


FIG. 4.— See the caption to Figure 5.

## GX 339-4 During Outburst Decline

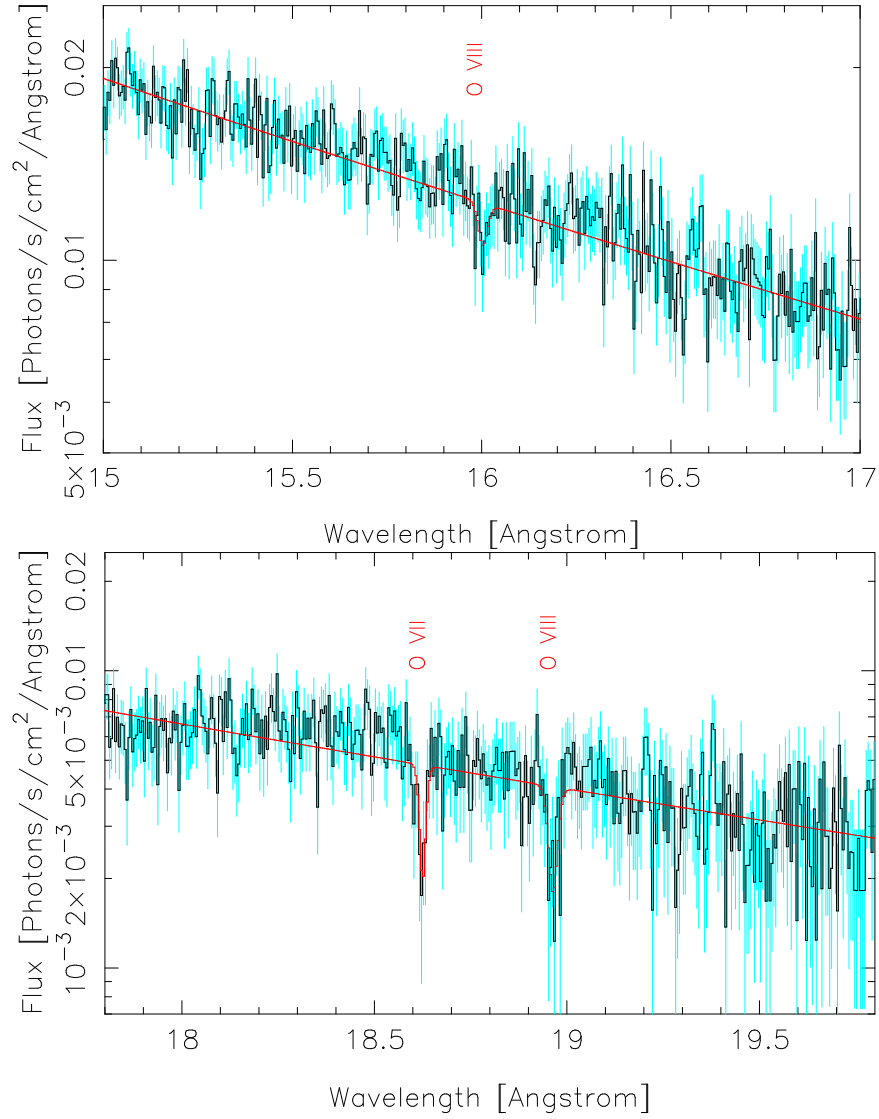


FIG. 5.— Slices of the combined first-order MEG spectra from GX 339-4, fit with simple power-law continua (modified by neutral ISM absorption edges where appropriate) and Gaussian line models in the wavelength regions shown. The best-fit model is shown in red, and  $1\sigma$  error bars are shown in blue. A number of resonance absorption lines, primarily from He-like and H-like species, are clearly detected and resolved. See Table 2 for line identifications and properties and Table 3 for line equivalent widths predicted by photoionized absorber models with varying.



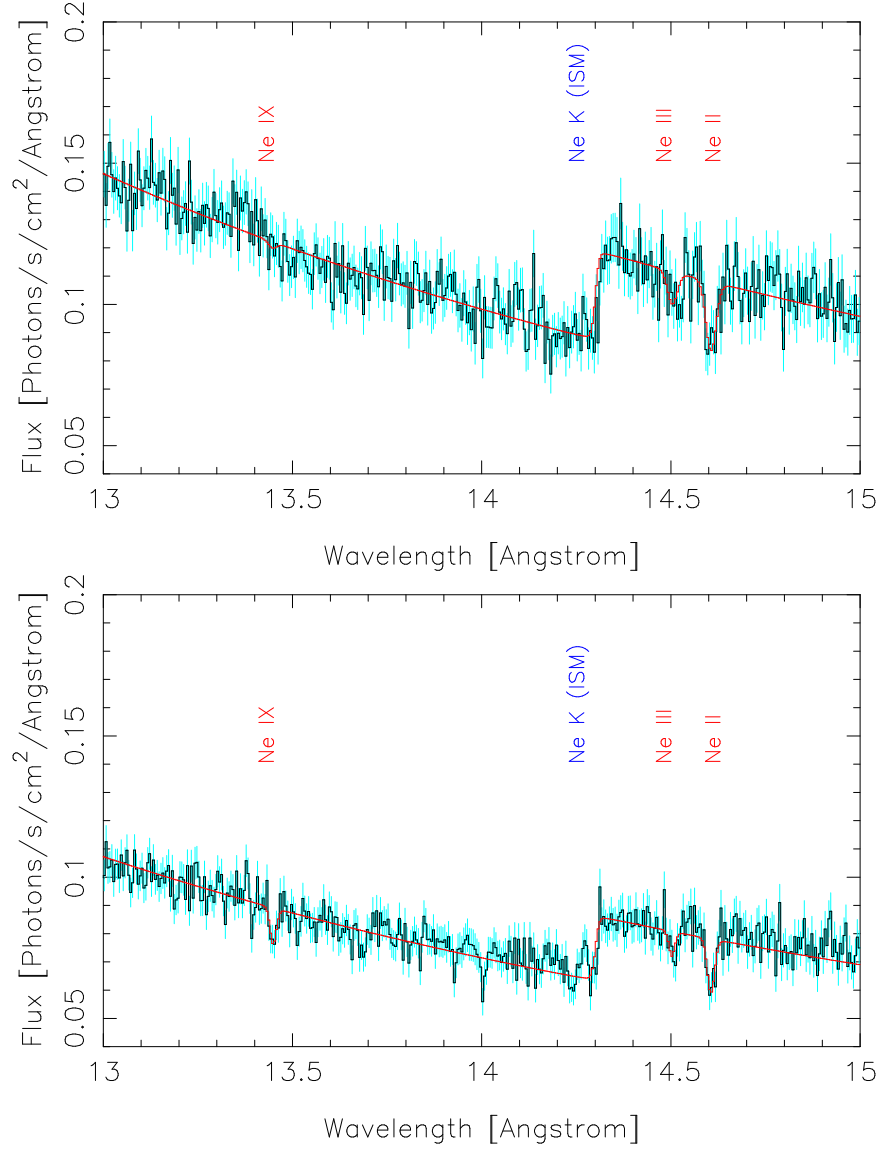


FIG. 6.— The Galactic black hole candidate XTE J1650–500 was observed on two occasions (30 ksec each) with the *Chandra*/HETGS 30 ksec *Chandra*/HETGS (Miller et al. 2002b). A slice of the MEG spectrum from the first observation is shown above, and the corresponding slice of the second observation is shown below. The spectra were fit with simple power-law models, modified by neutral ISM absorption edges and Gaussian line models. Note that the Ne IX line is not detected in the first observation, but that the Ne II line is quite strong. In contrast, the Ne IX line is detected in the second observation. The Ne II line is marginally stronger in the first observation; the Ne III resonance line is not clearly detected in either spectrum. The first observation occurred at a source flux of roughly 0.40 Crab and the second at a flux of roughly 0.25 Crab, 25 days after the first. This indicates that the absorbing geometry changed with time, linking the absorbing geometry to the accreting source instead of coronal gas in the ISM.